IAHR 2017

37th IAHR WORLD CONGRESS
13-18 August, 2017
Kuala Lumpur, Malaysia

COMBINED SEWER OVERFLOW (CSO) CONTROL

DISCHARGE CAPACITY OF JUNCTION MANHOLES WITH BOTTOM DROPS OR TOP OFFSETS

GAETANO CRISPINO[1], MICHAEL PFISTER[2] & CORRADO GISONNI[3]

[1,3] Department of Civil Engineering, Design, Building and Environment, University of Campania "Luigi Vanvitelli", Aversa (CE), Italy, gaetano.crispino@unina2.it; corrado.gisonni@unina2.it

[2] Civil Engineering Department, Haute Ecole d'Ingénierie et d'Architecture, Fribourg, Switzerland, michael.pfister@hefr.ch

ABSTRACT

An adequate operation of combined sewer systems is related to the efficiency of sewer manholes. Sometimes, sewer manholes are designed to convey safely storm water discharges with a return period shorter than the infrastructure life time. In other cases, the manhole discharge capacity is sufficient but the flow structure established in the manhole leads to unacceptable free-surface flow conditions. This poor performance may easily occur in junction manholes, which merge two or more upstream branches into a single downstream collector. The hydraulic behavior of junction manholes under sub- and supercritical flows has been thoroughly studied in the past, mainly on an experimental basis. However, former studies are all referred to a standard junction manhole layout, with a constant diameter assigned to both up- and downstream branches along with a flat manhole invert. Contrarily, diversified set-ups are usually employed in practical cases. Upstream sewer branches are generally characterized by various cross-section profiles. Moreover, the good design practice recommends settling the concerned branches by aligning the branch tops, in order to avoid backwater effects. Given the above, advancement in design procedures for junction manholes is strongly required, mainly with regard to the discharge capacity of junctions characterized by generalized configurations. The present study considers the results of experimental campaigns performed on different physical models of junction manholes. A communal structure with a junction manhole approached by two circular upstream branches, with variable diameters, is considered. Then, junction angles and upstream branch diameters are varied, resulting in different manhole set-ups with inlet bottom drops or top offsets. Selected overload experimental runs are performed to investigate the hydraulic conditions under which the manhole discharge capacity is exceeded. The analysis of the experimental data allowed in outlining a preliminary comparison of discharge capacity of junctions with generalized layouts.

Keywords: Hydraulic design; sewer manhole; junction manhole; supercritical flow; discharge capacity.

1 INTRODUCTION

Sewer systems operate satisfactorily when the performance of their collectors and manholes is hydraulically adequate. In particular, sewer manholes are crucial elements in urban drainage systems. Each hydraulic or geometrical alteration is located into sewer manholes. Simultaneously, the punctual variation of basic features as cross-section profile, hydraulic roughness, channel slope or discharge frequently can lead to the occurrence of undesired phenomena (shock waves, breakdowns etc.). An accurate design of sewer manholes is thus fundamental. If a sewer manhole does not function as required, then the free-surface conditions across the related collectors are probably unacceptable. Among others, junction manholes are the most frequent structures within urban drainage systems. They combine two or more upstream sewer branches into a single downstream collector, as often occurred into ramified drainage nets. The main component of a junction manhole is the junction chamber, inside of which the free-surface flow irregularities should to be opportunely restrained. The benches of the chamber are required to limit the shock wave maxima, whereas the discharge capacity of the overall structure should be larger than incoming storm water discharges in order to avoid manhole overflow phenomena.

The manhole geometry can be properly selected provided that the hydraulic features of approach flows are exhaustively recognized. In particular, plan outlines of junction manholes approached by subcritical flows should exclude specific appurtenances with sharp-crested geometries. These accessories facilitate the presence of large dead-flow zones originating excessive energy losses across the structure. The computation of the energy loss coefficients for subcritical junction manholes is accomplished by applying the momentum equation based on the similitude between free-surface flows running in the manhole and pressurized flows (Hager, 1987). The recourse of the classical energy head equation helps to predict the subcritical free-surface profiles over the manhole (Gisonni and Hager, 2012), instead.

The flow scenario is completely different for supercritical approach flows. Here, the main intent consists in preventing the interruption of the regular supercritical flow structure into the manhole. If otherwise happens,

unpleasant events with severe shock waves, breakdown of air-transport in the downstream collector or choking flow in one or both the upstream branches can happen. If the height of the bench walls is safely chosen, then the shock wave maxima, even if significant, should not arise in particular care. According to main literature studies (Del Giudice and Hager, 2001; Gisonni and Hager, 2002; Crispino et al., 2016), the prediction of wave maximum heights is fulfilled by applying empirical relationships validated by physical model data. However, if the total discharge Q exceeds a given value, from here on out named as manhole discharge capacity, then the above-mentioned phenomena may occur resulting in a junction manhole failure.

As for the shock wave heights, the discharge capacity of supercritical junction manholes is estimable through experimental expressions (Del Giudice and Hager, 2001; Gisonni and Hager, 2002; Saldarriaga et al., 2017). This formula depends on the specific junction flow scenario (approach supercritical flows or mixed regimes with sub- and supercritical flows approaching the manhole all at once). In addition, the empirical relationships are all presented for a standard junction manhole set-up, characterized by circular upstream branches and a downstream collector with same diameter D. Moreover, the manhole inlets and outlet were always aligned. Nevertheless, this standardized set-up is a long way to be found in practical wastewater applications, given the enormous variety of geometrical configurations to be considered. Furthermore, a good practical rule commonly employed in the sewer collector design suggests aligning the tops of sewer branches entering and outing from manhole. A such farsightedness might avoid the formation of hydraulic jumps for backwater flows.

Given the above, existing equations valid for predicting the junction, manhole discharge capacity need to be validated, or modified if necessary, by considering generalized manhole set-ups. At this aim, the present paper provides first results derived by a set of experimental studies on 45° and 90° junction manholes, which were characterized by upstream branch diameters different from the downstream one and, above all, by the presence of small drops or top offsets at the manhole inlets.

2 PHYSICAL MODEL INVESTIGATION

Experiments were conducted at the Laboratory of Hydraulic Structures of the École Polytechnique Fédérale de Lausanne, Switzerland. Two physical models of junction manholes characterized by conventional dimensions were utilized, with a junction angle δ equal to 45° and 90°, respectively. As visible in Figure 1, the physical models were made out of PVC, with transparent conduits and manhole bench walls to facilitate the free-surface flow observations. Both 45° and 90° junction manholes were approached by two circular upstream branches, the straight (subscript o) and the lateral (subscript L) one. A downstream collector (subscript d), with a circular cross-section profile too, outed from the junction chamber. The diameter of the downstream collector was constant (D_d = 0.240m). Conversely, the upstream branches were characterized by variable diameters D_o and D_L, alternatively equal to $0.51 \cdot D_d$, $0.79 \cdot D_d$ and $1.00 \cdot Dd$. Nine set-up combinations resulted from the variation of the upstream branch diameters, as illustrated in Table 1. Set-up I was characterized by equal up- downstream diameters, corresponding to the standardized junction manhole layout.

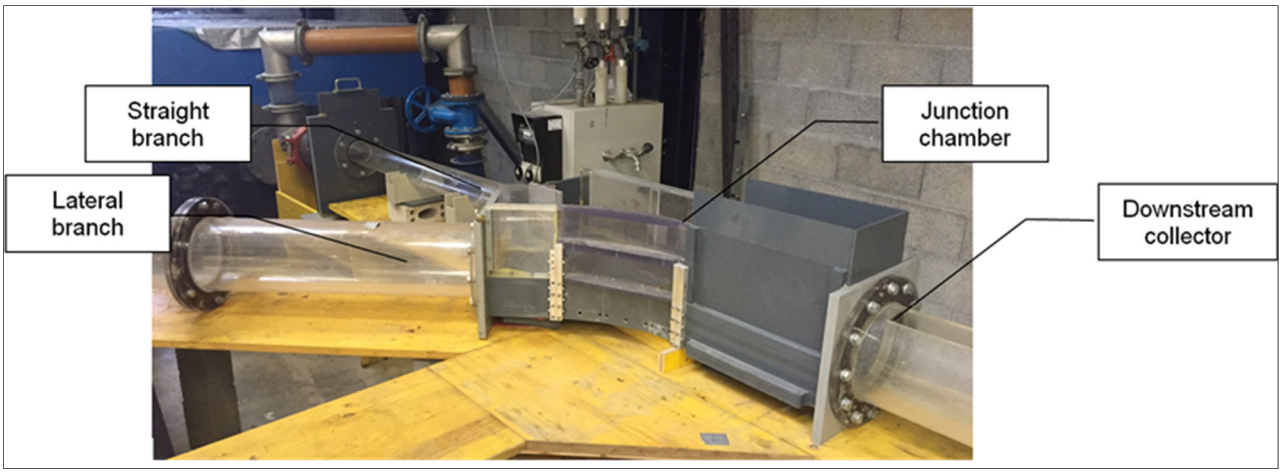

Figure 1. Physical model of 45° junction manhole installed at the LCH/EPFL.

Junction chamber and downstream collector inverts were always aligned. Bottom drops or top offsets (Figure 2) were thus present at the straight and/or at the lateral manhole inlet if the corresponding upstream branch diameter differed from the downstream one. In particular, the 45° junction manhole model was tested for both set-ups with bottom drops and top offsets, whereas the manhole inlets of the 90° junction manhole were only characterized by top offsets. The geometrical features of remaining components (lateral branch curvature, bench heights and junction chamber length) followed from the basic recommendations derived by Del Giudice and Hager (2001) and Gisonni and Hager (2002).

Table 1. Junction manhole set-ups tested by varying the upstream branch diameters (D_d = 0.240m).

Set-up	D_o [m]	D_o/D_d [-]	D_L [m]	D_L/D_d [-]
A	0.123	0.51	0.123	0.51
B	0.123	0.51	0.190	0.79
C	0.123	0.51	0.240	1.00
D	0.190	0.79	0.123	0.51
E	0.190	0.79	0.190	0.79
F	0.190	0.79	0.240	1.00
G	0.240	1.00	0.123	0.51
H	0.240	1.00	0.190	0.79
I	0.240	1.00	0.240	1.00

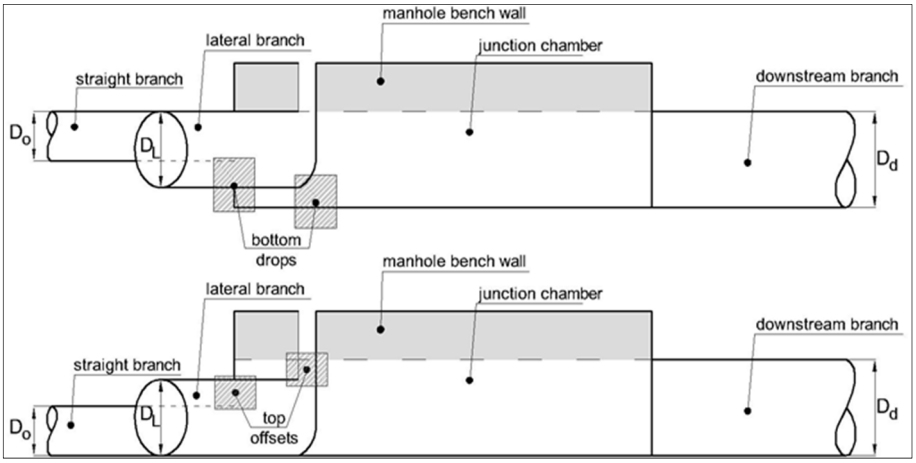

Figure 2. Sketch of the junction manhole with bottom drops (top) or top offsets (bottom).

Water depths, at fixed points along the conduits and the manhole, and shock wave heights, where waves occurred, were measured by the utilization of a conventional point gauge. The approach discharges Qo and QL were measured singularly by inductive flowmeters with a full scale (FS) accuracy of ±0.5%. Selected test-runs were carried out by varying the main hydraulic independent parameters for each upstream branch, including: the approach filling ratio Y = h/D, where h is the water depth, and the approach flow Froude number $F = Q/(gY^4h^5)^{0.5}$ (Pfister and Gisonni, 2014), where Q is the discharge and g is the gravitational acceleration. The approach filling ratios varied between 0.20 and 0.65, because for supercritical flows in circular conduits the free surface flow breaks down whenever the filling ratio is larger than 70% (Hager and Gisonni, 2005). Different junction flow scenarios, with approach flows simultaneously supercritical or subcritical or under mixed flow conditions, were replicated in the physical model. However, transcritical flows with Froude numbers ranging between 0.80 and 1.20 (Gisonni and Hager, 2012) were avoided, so that only fully sub- or supercritical flows entered the junction manhole.

3 JUNCTION MANHOLE DISCHARGE CAPACITY

As specified by Del Giudice and Hager (2001), the discharge capacity (subscript C) of a junction manhole can be exceeded due to the occurrence of two possible troubling phenomena:

- choking flow in the downstream collector, occurred due to the formation of a relevant swell up to occlude the manhole outlet cross-section. If the approach flows are both supercritical, then they break down with an abrupt transition from free-surface to pressurized air – water flow;
  choking of one or both the approach flows over the upstream branches, which may potentially happen when the upstream flows are so perturbed to break the free-surface flow regime or for an approach flow significantly dominant on the other one. In both cases, a hydraulic jump occurs with a possible backwater effect. The pressurization of an upstream branch may successively cause the breakdown condition in the junction manhole.

The junction discharge capacity is usually represented by means the capacity Froude number $F_C = Q_C/(g \cdot D^5)^{0.5}$ (Del Giudice and Hager, 2001). A set of experimental relationships was suggested by Del Giudice and Hager (2001) and Gisonni and Hager (2002) to predict the capacity discharge of standard 45° ad 90° junction manholes, depending on the specific flow scenario. These relationships are summarized in Table 2. As reported, the capacity Froude number is fixed as a function of the approach filling ratio Y_o and Y_L. According to the concerned formula, the straight filling ratio Y_o has a more significant effect. Furthermore, for

junction flow scenarios (III) (δ =45°) and (I) (δ =90°), the straight Froude number F_o was also included among the affecting parameters.

Table 2. Experimental relationships used for predicting F_C in 45° or 90° junction manholes under a standard set-up (Del Giudice and Hager, 2001; Gisonni and Hager, 2002).

		Junction flow scenario	Experimental relationship
45° junction manhole	(I)	both supercritical flows	$F_C = 5.5 \cdot Y_o \cdot Y_L^{0.5}$
	(II)	subcritical straight flow and supercritical lateral flow	$F_C = 0.7 \cdot (Y_o \cdot Y_L^{0.5})^{1/3}$
	(III)	supercritical straight flow and subcritical lateral flow	$F_C = 0.6 \cdot Y_o \cdot F_o$
90° junction manhole	(I)	both supercritical flows	$F_C = 0.6 \cdot F_o \cdot Y_o^{1.2} \cdot Y_L^{-0.2}$

3.1 45° junction manholes

The experimental campaign conducted on the 45° junction manhole with inlet top offsets (Niedermann, 2013) was characterized by particular tests during of which the capacity of the structure was clearly overtaken. A choking flow was observed in the junction chamber, and it was essentially induced by the formation of limit flow conditions over the upstream branches. The pressurization of one or both upstream branches provoked the occurrence of a hydraulic jump in the manhole or just upstream from the junction chamber. An increase of the water level up to the crest of the manhole bench walls was thus observed. Contrarily, the choking flow in downstream collector was hardly reproducible experimentally, because the large downstream collector diameter (D_d = 0.240m) compared with the smaller upstream branch diameters would have required significant tailwater levels to produce the transition from free-surface to pressurized flow. However, these water levels were difficult to be obtained by installing small upstream branch diameters.

For 45° junction manholes equipped with bottom drops (Crispino, 2016), the discharge capacity was again exceeded due to the abrupt pressurization of the upstream branches. Figure 3 shows the alarming overflow condition observed in the junction chamber during a specific test-run. Approach flows were both supercritical, with Froude numbers equal to F_o = 1.49 and F_L = 3.96, and the corresponding filling ratios were forced to be Y_o = 0.60 and Y_L = 0.40. The development of unstable free-surface flow conditions over the lateral branch generated, firstly, the transition to a pressurized flow along the pipe and, at a later time, the propagation of the choking flow in the junction chamber and along the straight branch. The bottom drop at the straight inlet did not thus inhibit the backwater effect into the straight branch. As a result, the water level in the junction chamber touched lightly the crest of the bench walls, as visible in Figure 3. The outlet cross-section was thus completely submerged, and a gated flow occurred at the entrance of the downstream collector.

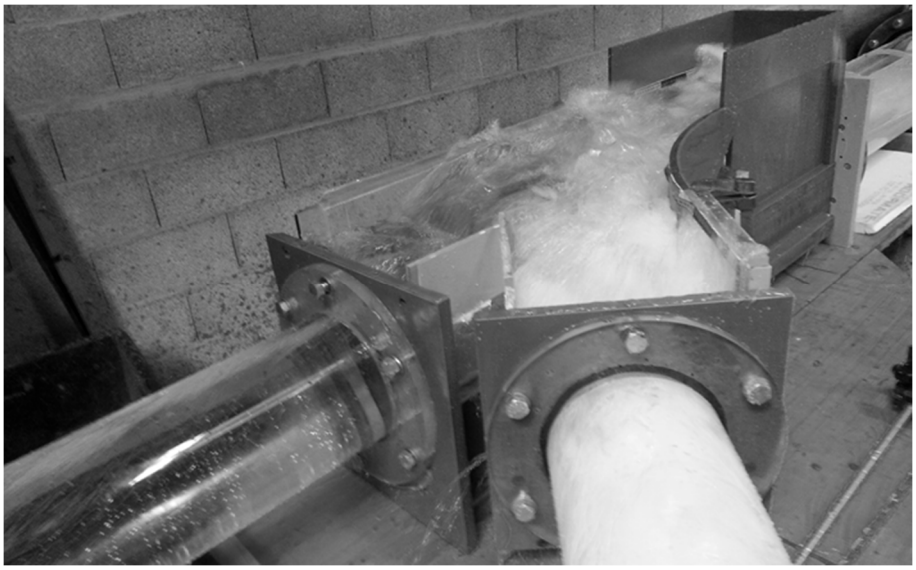

Figure 3. Choking of the junction manhole due to the abrupt pressurization of upstream branches, as observed in 45° junction manhole with bottom drops under set-up E (see Table 1).

As previously observed by Del Giudice and Hager (2001) for standardized 45° junctions, the experimental discharge capacity F_c can be plotted against $Y_o \cdot (Y_L)^{0.5}$, for flow scenarios (I) and (II), and against $Y_o \cdot F_o$, when the hydraulic behavior of the junction manhole is dominated by the straight supercritical flow (flow scenario (III)). However, the experimental data collected for 45° junction manholes under generalized set-ups

did not follow the recommended equations, as represented in Figure 4a. The variation of the upstream branch diameters had to be thus accounted for because it made the experimental relationships suggested by Del Giudice and Hager (2001) ineffective. Given that the downstream collector diameter D_d was unchanged passing from standardized to generalized junction manholes, it is convenient to introduce the diameter ratio $\beta = D_i/D_d$ (i = o, L) to consider the variability of the upstream branch diameters. Figure 4b shows the experimental capacity Froude numbers F_C as a function of $\beta_o Y_o \cdot (\beta_L Y_L)^{0.5}$. For upstream branch diameters equal to the downstream one, the diameter ratio coefficients β_o and β_L are equal to 1.0 giving again the parameter suggested by Del Giudice and Hager (2001). Conversely, if the upstream branch diameters differ from the downstream one, then the conventional equation can be modified as:

$$F_C = 5.5 \cdot \left[\beta_o Y_o \cdot \left(\beta_L Y_L \right)^{0.5} \right] \quad [1]$$

As visible, Eq. [1] overestimates the discharge capacity exhibited by 45° junctions with bottom drops or top offsets, especially when the lateral diameter is $D_L = 0.51 \cdot D_d$ (set-ups (A) and D)). No evident differences between junction manholes equipped with bottom drops or top offsets are recognized, instead. It is noteworthy that the experimental data corresponding to the set-up (I), that is the standard junction set-up, are well predicted by Eq. [1].

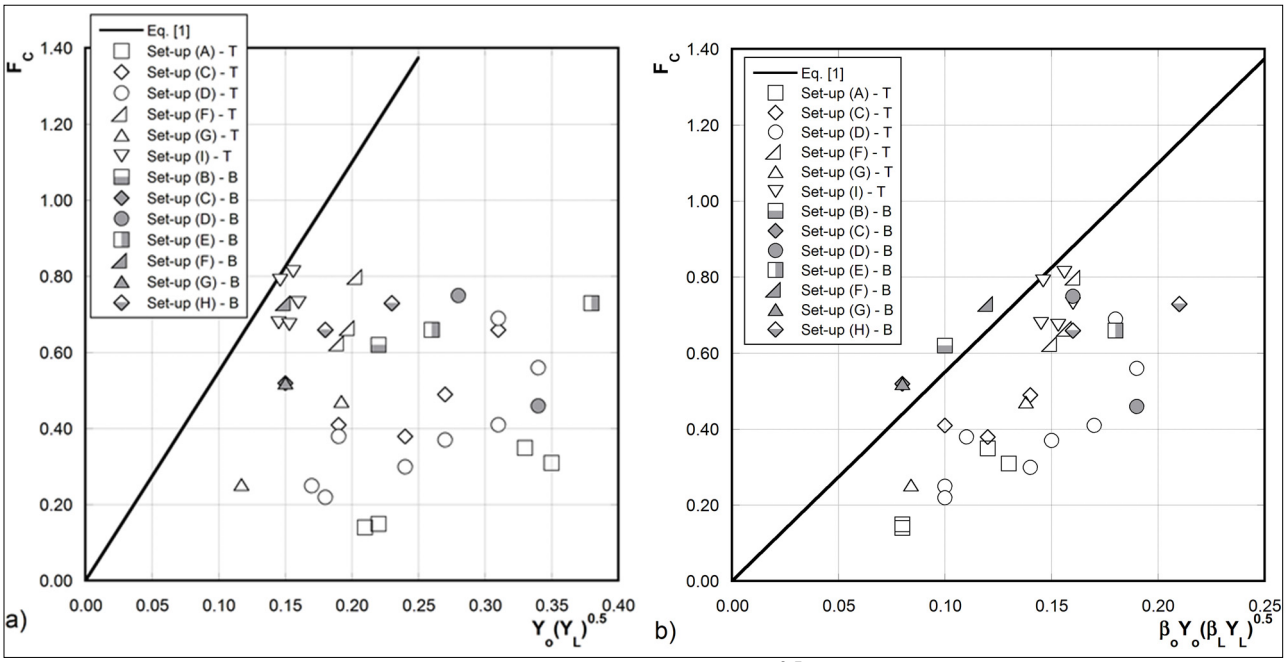

Figure 4. Capacity Froude Number F_c as a function of $\beta_o Y_o \cdot (\beta_L Y_L)^{0.5}$ for 45° junction manholes equipped with bottom drops (B) or top offsets (T) under junction flow scenario (I).

For subcritical flows issued by the straight or the lateral branch (junction flow scenarios (II) and (III)), the capacity Froude number of 45° junction manholes can be plotted against $[\beta_o Y_o \cdot (\beta_L Y_L)^{0.5}]^{1/3}$ and $(\beta_o Y_o F_o)$ (Figures 5a, b), respectively, according to following equations:

$$F_C = 0.7 \cdot \left[\beta_o Y_o \cdot \left(\beta_L Y_L \right)^{0.5} \right]^{1/3} \quad [2]$$

$$F_C = 0.6 \cdot \left(\beta_o Y_o F_o \right) \quad [3]$$

Here, only experimental data referred to the junction manhole equipped with top offsets are available. Physical observations confirm previous statements derived by Del Giudice and Hager (2001). The discharge capacity of 45° junction manholes under junction flow scenario (III) is larger than under flow scenario (II), even if generalized set-ups with variable upstream branch diameters are considered. As illustrated in Figures 5a, b, the relationships suggested by Del Giudice and Hager (2001), even if modified by introducing the diameter ratio, don't allow to estimate accurately the discharge capacity of 45° junction manholes with top offsets at manhole inlets. The discrepancies are more evident when junction flow scenario (II) is considered (Figure 5a). In this case, the effect related to the reduction of the lateral branch diameter is again significant, as recognized for the flow scenario (I). Infact, the differences between observed and predicted data are larger than for other set-ups. If junction flow scenario (III) is considered (Figure 5b), then the reliability of the expression suggested

for standard junction manholes increases. This evidence might prove that larger deviations between the experimental data collected for generalized junction manholes and the relationships recommended by Del Giudice and Hager (2001) for standard junctions are derived when supercritical flows are issued by the lateral branch.

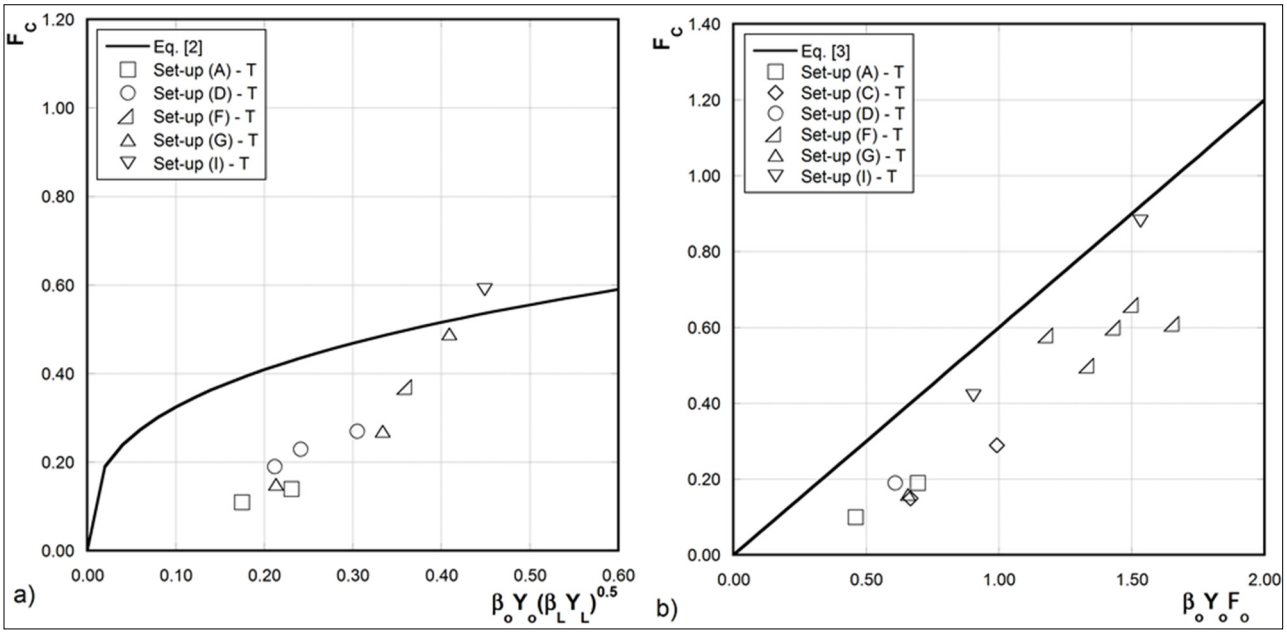

Figure 5. Capacity Froude Number F_c as a function of: a) $\beta_o Y_o(\beta_L Y_L)^{0.5}$ (junction flow scenario II) and b) $\beta_o Y_o F_o$ (junction flow scenario III) for 45° junction manholes equipped with top offsets.

3.2 90° junction manholes

Gisonni and Hager (2002) experienced the discharge capacity excess of 90° junction manholes because of the formation of a relevant swell height. The swell gave origin to the occurrence of the choking of the downstream collector. More rarely, the junction discharge capacity was overtaken due to the flow blockage in the upstream branches. Gökok (2013) investigated the discharge capacity of 90° junction manholes equipped with inlet top offsets originated by upstream branch diameters different from the downstream one. As for Niedermann (2013), the overflow condition in the junction chamber was mainly due to the pressurization of one or both the upstream branches. The choking of the downstream collector induced by the formation of a relevant swell at the manhole outlet was not frequent because of the reduced upstream branch diameters which inhibited the achievement of significant tail water depths.

For 90° junctions under junction flow type (I), Gisonni and Hager (2002) concluded that the capacity Froude number F_c depended on the dynamic momentum of the straight flow F_oY_o multiplied for the ratio Y_o/Y_L (see Table 2). However, as for 45° junction manholes, the reduction of the upstream branch diameters affected the experimental capacity Froude numbers observed by Gökok (2013). Contrarily, if the diameter ratios β_o and β_L are again adopted, then the following equation can be used:

$$F_C = 0.6 \cdot \left[F_o \cdot \left(\beta_o Y_o / \beta_L Y_L \right)^{0.2} \right] \qquad [4]$$

The experimental data collected for 90° junction manholes with inlet top offsets result to be nearby located around the line expressed by Eq. [4], as represented in Figure 6. Again, more relevant deviations between observed and predicted capacity Froude numbers are mostly obtained for the smallest lateral branch diameter D_z/D_d = 0.51. Moreover, similarly to 45° junction manholes the employment of the empirical formula adopted for the standard junction manhole continues to give overstimated discharge capacity values.

Differently from Gisonni and Hager (2002), Gökok (2013) tested the capacity of the physical model of 90° junction manhole also under subcritical approach flows (junction flow scenarios (II) and (III)). Figures 7a, b shows the corresponding results. For such junction flow types, the capacity Froude numbers are hereby estimated by using Eq. [2] and [3] according to the recommendations for 45° junction manholes. The discharge capacity of the 90° junction manhole approched by a supercritical straight flow and a subscritical lateral flow results to larger than in the reverse junction flow type, as identified previously for 45° junction manholes.

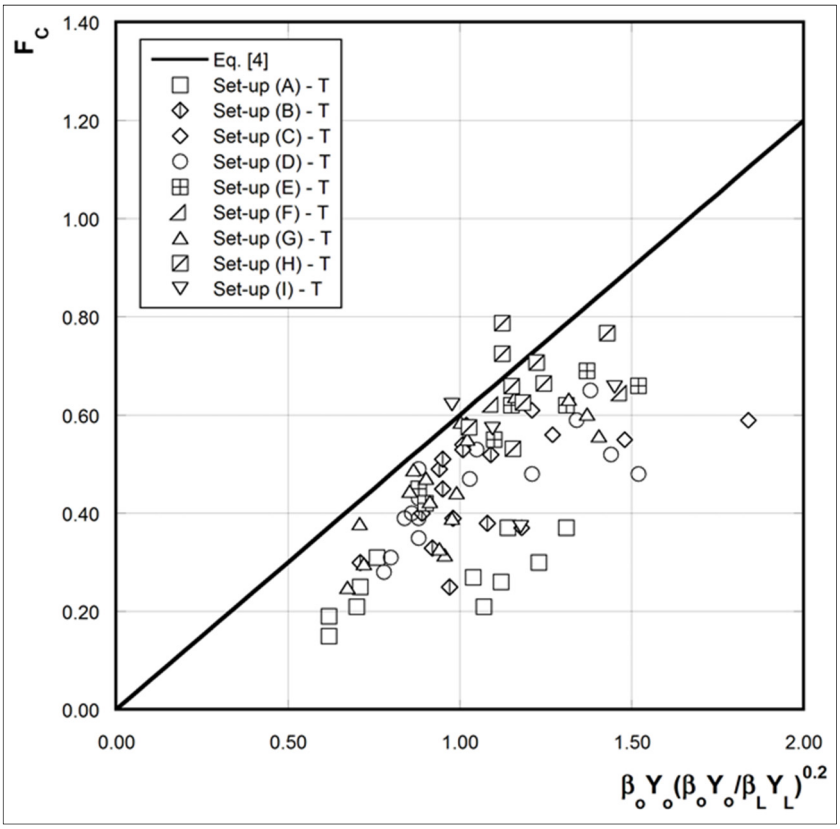

Figure 6. Capacity Froude Number F_c as a function of $\beta_o Y_o(\beta_o Y_o/\beta_L Y_L)^{0.2}$ for 90° junction manholes equipped with top offsets (T) under junction flow scenario (I).

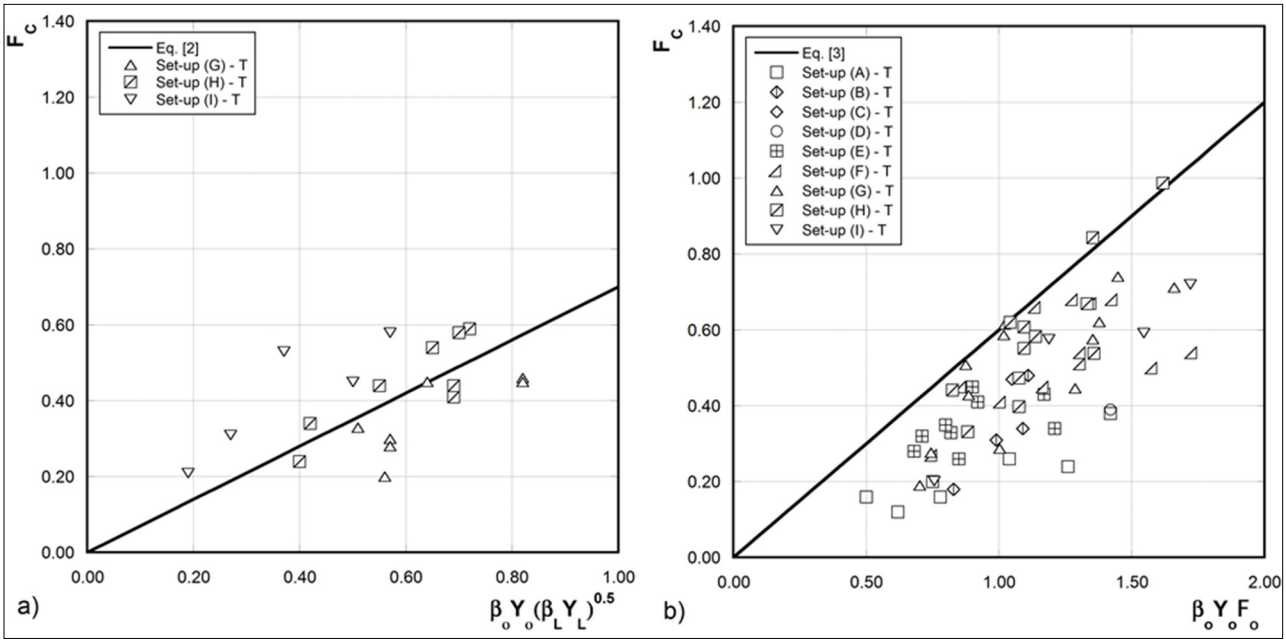

Figure 7. Capacity Froude Number F_c as a function of: a) $\beta_o Y_o \cdot (\beta_L Y_L)^{0.5}$ (junction flow scenario II) and b) $\beta_o Y_o F_o$ (junction flow scenario III) for 90° junction manholes equipped with top offsets.

4 FILLING RATIO IN THE DOWNSTREAM COLLECTOR

As described above, the overload condition resulting in the excess of the discharge capacity of the 45° and 90° junction manholes were initiated by the instable free-surface flow conditions in the upstream branches. A hydraulic jump thus occurred in the junction chamber, and the water level increased significantly up to crest of the manhole bench walls in the worst-case scenario. As a consequence, the junction flow generated a wall shock wave which impinged abruptly on the manhole end wall as represented in Figure 8.

The outlet cross-section resulted to be occluded and, in most cases, a gated flow entered the downstream collector.

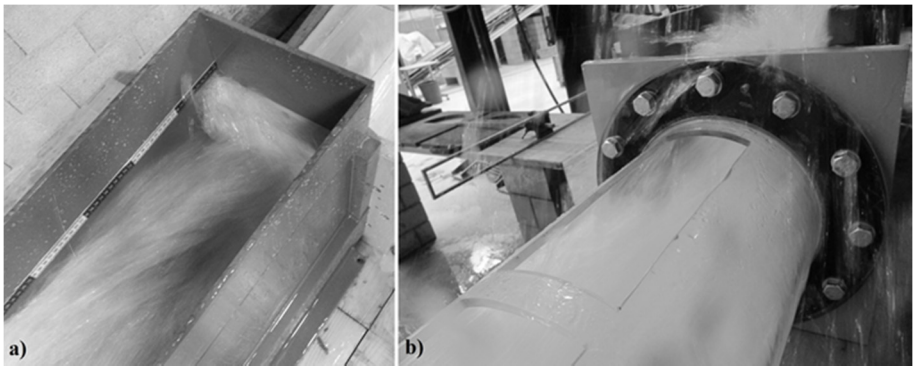

Figure 8. Top a) and downstream b) view of the flow impact against the manhole endwall, as observed during the physical model tests on the 45° junction manhole with bottom drops.

The free-surface flow running along the downstream collector was relevantly shocked (Figure 9a), and it resulted to be transcritical (F_d < 1.20) or, sometimes, weakly supercritical (1.20 < F_d < 2.00). The experimental filling ratio Y_d ranged between about 0.25 and 0.75, depending on the severity of the overflow phenomenon occurred in the junction chamber. Figure 9b reports the downstream Froude numbers, as a function of the total discharge $Q = Q_o + Q_L$, against the downstream filling ratios, and it compares the present results with the observations collected by Saldarriaga et al. (2017) on a physical model of supercritical junction manhole approached by three upstream branches. As can be seen, downstream Froude numbers obtained by Saldarriaga et al. (2017) (grey circles in Figure 9b) were always less than 1.0 (subcritical flows) whereas the outflow observed in the present investigation was supercritical.

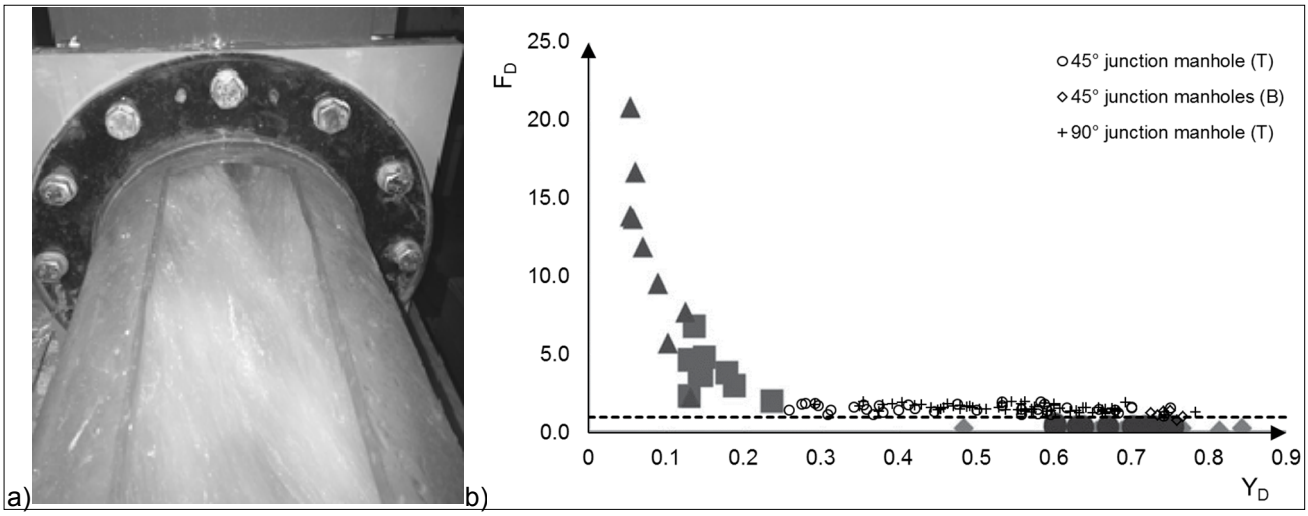

Figure 9. a): Downstream view of the outflow during an overload test on the 45° junction manhole with bottom drops and b) Froude numbers F_d as a function the downstream filling ratio Y_d (grey triangles and squares correspond to the upstream filling ratios observed by Saldarriaga et al., 2017).

5 CONCLUSIONS

The computation of the discharge capacity of junction manholes is a basic phase in the design of such hydraulic structures, especially when approach supercritical flows are expected. The main equations suggested in literature are all referred to a standard junction manhole set-up. However, this reference geometry is often in unconformity with the real junction configurations. The present study aimed thus to verify the reliability of concerned relationships for generalized junction layouts characterized by variable upstream branch diameters and, above all, by the alignment of the branch tops.

Preliminary results derived by the overload test on 45° and 90° junction manholes equipped with bottom drops or top offsets showed that the conventional equations used for predicting the capacity Froude number under various junction flow types are not reliable. Contrarily, it was necessary to introduce the diameter ratio in these empirical equations accounting for the variation of the upstream branch diameters. As modified, the new relationships are characterized by a larger accuracy, even if they overestimated the experimental data.

No significant difference between the discharge capacity of junction manholes with bottom drops or top offsets emerged according to the present observations.

The excess of the discharge capacity of both 45° and 90° junction was due to the occurrence of choking flow in the upstream branches. In most cases, the overflow of the junction chamber happened, and a gated flow entered the downstream collector. Despite the shock effects, the free-surface flow along the downstream collector was transcritical or, sometimes, supercritical, differently from Saldarriaga et al. (2017).

REFERENCES

Crispino, G., Pfister, M. & Gisonni, C. (2016). Shock Wave Patterns in Supercritical Junction Manholes with Inlet Bottom Offsets, *Proceedings of the 4th IAHR Europe Congress*, Liege, Belgium, 27-29 July, 563-570.

Del Giudice, G. and Hager, W.H. (2001). Supercritical Flow in 45° Junction Manhole. *Journal of Irrigation Drainage Engineering*, 127(2), 100-108.

Gisonni, C. & Hager, W.H. (2002). Supercritical Flow in the 90° Junction Manhole. *Urban Water,* 4(4), 363-372.

Gisonni, C. & Hager, W.H. (2012). *Idraulica dei Sistemi Fognari – Dalla Teoria alla Pratica*, Springer-Verlag, 625.

Gökok, T. (2013). Physical Model Investigation of Supercritical Flow in Junction Manholes, *MSc. Thesis.* Laboratory of Hydraulic Constructions (LCH), Ecole Polytechnique Fédérale de Lausanne (EPFL), Lausanne, Switzerland.

Hager, W.H. (1987). Discussion to Separation Zone at Open-Channel Junctions. *Journal of Hydraulic Engineering*, 113(4), 539-543.

Hager; W.H. & Gisonni, C. (2005). Supercritical Flow in Sewer Manholes. *J. Hydraul. Res.*, 43(6), 660-667.

Niedermann, E. (2013). Physical Model Investigation of Supercritical Flow in 45° junction manholes, *MSc. Thesis*. Laboratory of Hydraulic Constructions (LCH), Ecole Polytechnique Fédérale de Lausanne (EPFL), Lausanne, Switzerland.

Pfister, M. & Gisonni, C. (2014). Head Losses in Junction Manholes for Free Surface Flows in Circular Conduits. *Journal of Hydraulic Engineering*, 140(9).

Saldarriaga, J., Rincon, G., Moscote, G. & Trujillo, M. (2017). Symmetric Junction Manholes under Supercritical Flow Conditions. *Journal of Hydraulic Research*, 55(1), 135-142.

Proceedings of the 37th IAHR World Congress
August 13 – 18, 2017, Kuala Lumpur, Malaysia

A FINITE VOLUME APPROACH FOR TRANSIENT FLOW IN URBAN STORMWATER DRAINAGE SYSTEM CONTAINING TRAPPED AIR

LING ZHOU[1], ALAIN JOËL ELONG[2], XU YANG[3], HUAN WANG[4] & TIANWEN PAN[5]

[1, 2, 4, 5] College of Water Conservancy and Hydropower Engineering, Hohai University, Nanjing, China, zlhhu@163.com; alainjoel.elong@yahoo.fr; wanghuan0527@163.com; monamourzhu@163.com

[3] China Water Resources Beifang Investigation, Design and Research Co. Ltd. (BIDR), Tianjing, China, yangxu629730@163.com

ABSTRACT

Flow transients of air-water interactions in urban stormwater drainage systems under rapid flow surcharging conditions were investigated. First-order Finite Volume Method (FVM) Godunov-type scheme was developed to handle air-water problem in a rapid filling closed-end pipeline with tail water. The exact Reimann solution was introduced to provide the fluxes at grid interface in water region. The air-water interface was tracked by Godunov-type schemes coupled with ideal air law. The pressure results predicted by the proposed FVM model were compared with the experimental data and the results from the previous elastic model with fixed-grid Method of Characteristics (MOC) scheme. Comparisons show that the proposed model is successful in simulating transient pressure. Moreover, the first-order FV model and the MOC model could obtain the consistent simulation results, since the two models have the same first-order accuracy.

Keywords: Urban stormwater drainage systems; transient flow; trapped air; computation.

1 INTRODUCTION

The main component of urban stormwater drainage systems is a system of pipes that collects storm run-off and distributes the runoff to points of treatment or disposal. However, hydraulic failures in urban stormwater systems, such as manhole cover blow off, geysers, combined sewer overflows, and street and basement flooding, are common in most of the cities. Particularly, rapid urbanization, extreme rainfall over return period and drainage-storage combination of “Sponge City”, induce that the problems described above occur frequently recently. It is urgent to understand well the mechanisms leading to failures in the design of new drainage systems and the rehabilitation of aging drainage infrastructures.

Transient behaviors and mechanisms of hydraulic failures in drainage systems are very complicated and still limited. Previous published studies indicated that, high pressure surges induced by air entrapment and air release may be one of the important factors causing hydraulic failures in pipelines. The few video records of hydraulic failures, such as those from Minneapolis, U.S.A. (Figure 1(a)) and Montreal, Canada (Figure 1(b)), clearly show that before a manhole cover was blown off, a loud air noise was heard under the manhole cover and the cover was bouncing up and down, which indicates air compression and expansion inside the system. Moreover, a sudden transient of the entrapped air pocket in a dead-end pipe may induce high-pressure surges leading to deformations or even pipe failure (Wylie et al., 1993; Hou et al., 2014). So far, many pipe incidents and accidents occur due to the fast-multi-phase fluid transients, and there is still much work for the special transient flow (BHR, 2015).

(a) Minneapolis, USA, 1999 (b) Montreal, Canada, 2011

Figure 1. Video records of geyser in urban stormwater drainage system.

Most of the existing mathematical models simulating the rapid filling with entrapped air pocket are one dimensional (1D), including either an elastic-water model with fixed-grid Method of Characteristics (MOC) scheme (Liu et al., 2011; Zhou et al., 2011a; 2013a; 2013b; 2013c; 2013d) or a rigid-water column model (Martin, 1976; Cabrera et al., 1992; Izquierdo et al., 1999; Zhou et al., 2002). Compared with the elastic model,

the rigid model is fast and efficient, avoiding interpolation problems of tracking the air-water interface. However, it is found that the rigid column theory breaks down for systems with small air pockets, while the water hammer theory shows fairly good overall agreement with the tests (Lee and Martin, 1999; Zhou et al., 2011a; Malekpour, 2014). In order to avoid interpolation problems of tracking the air-water interface by using the fixed-grid MOC scheme, the authors (Liu et al., 2011; Zhou et al., 2011a) developed the rigid-plug or virtual-plug elastic-water model, which can reach to the same accuracy with the complete elastic-water model. In addition, the authors (Zhou et al., 2011b) firstly introduced the two- and three-dimension Volume of Fluid (VOF) method to simulate transient flow during the filling process in a confined pipe system.

Finite Volume Method (FVM) has been widely used in the solutions of hyperbolic systems, such as gas dynamics and shallow water waves [see recent books by Toro (2009)]. FVMs are noted for their ability to (i) conserve mass and momentum, and (ii) provide sharp resolution of discontinuities without spurious oscillations. In addition, FVMs, which are essentially based on the application of the physical laws to a control volume, provide correct jump relations at discontinuities (Toro, 2009). A few researchers (Guinot, 2001; Hwang and Chung, 2002; Zhao and Ghidaoui, 2004; León et al., 2006; 2010) attempted to apply the FVM to water hammer problems in single water phase flows or the transient-mixed flows. At present, the application of the FVM is rare to model the air-water problem in rapid filling pipe with tail water.

In this paper, FVM Godunov-type scheme was developed to handle the air-water problem in the rapid filling pipeline with initial tail water. To date, the existing MOC model (Zhou et al., 2013d) is limited to first-order accuracy. In order to compare with the previous elastic water model in the same order accuracy, the first-order explicit FVM Godunov-type scheme is introduced here. An experimental setup of rapid filling pipe with tail water and entrapped air pocket was designed to validate the proposed model. The comparisons of first-order scheme and the fixed-grid MOC scheme were also conducted. Finally, the results are summarized in the Conclusion.

2 MATHEMATICAL MODELS

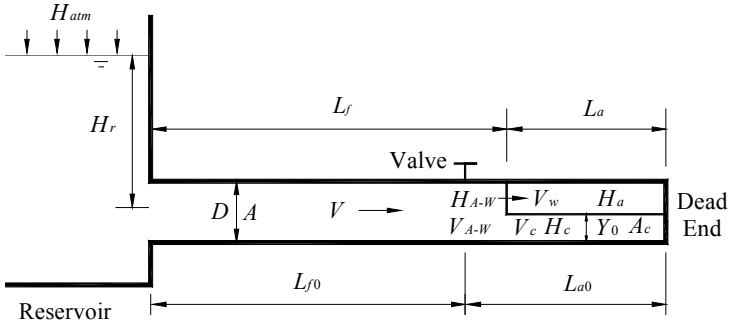

Figure 2. Schematic of filling partially full pipe with dead end.

Figure 2 shows configuration of pipe system, which consists of a source reservoir, an upstream water column, a valve, a downstream water column, with an entrapped air pocket and air water interface. H_r is the upstream (gauge) head. H_{atm} is atmospheric pressure. D is the pipe diameter and is constant for all sections. A is cross-sectional area of pipe section (m^2). L_f is the water column length at t time, and L_{f0} is the initial value (t=0). H_a, and L_a are respectively absolute pressure head (m) and length of entrapped air pocket at t time, and their initial value are H_{a0} and L_{a0}. V is the water velocity. $V_{A\text{-}w}$ and $H_{A\text{-}w}$ are the velocity and pressure head of the filling water at the air-water interface. V_w and V_c are the velocities of the surge front and tail water at the air-water interface. Y_0 and A_c is initial depth and cross-sectional area of tail water.

In the simulation of rapid filling, the following assumptions were introduced in the development of one dimension mathematical model (Zhou et al., 2013a; 2013b): (1) the air-water interface between the filling water and entrapped air pocket is perpendicular to the centerline of pipe in the whole filling process; (2) the pipe friction factor is considered as constant; (3) the entrapped air pocket is treated as ideal gas; and (4) there is no heat and phase exchange between the air and water phase. In order to include the effect of tail water (as shown in Figure 2), some additional assumptions are necessary (Zhou and Liu, 2013): (5) the depth of tail water beneath the entrapped air pocket is constant; (6) when the entrapped air is compressed, the tail water where the filling water reaches will become filling water; and (7) for the air expanding process, the tail water length increases with the upstream movement of the air-water interface.

The water part consists of filling water and tail water. In the tail water region, the water length changes with the movement of filling water while the depth is always kept constant based on the assumptions. The continuity and momentum equations are applied to the filling water region (Wylie et al., 1993):

$$\frac{\partial H}{\partial t} + V\frac{\partial H}{\partial x} + \frac{a^2}{g}\frac{\partial V}{\partial x} = 0 \qquad [1]$$

$$\frac{\partial V}{\partial t} + V\frac{\partial V}{\partial x} + g\frac{\partial H}{\partial x} + \frac{f|V|V}{2D} = 0 \quad [2]$$

As shown in Eq. [1] and [2], the nonlinear convective terms V∂H/∂x and V∂V/∂x were included to investigate their effects on the transient pressure during the rapid filling, which rarely were considered in the previous numerical simulations. In this paper, the nonlinear convective terms were considered in the model development. However, in order to compare the existing model, the nonlinear convective terms were neglected in the comparison simulations.

The equation for the air phase is:

$$H_a V_a^m = H_{a0} V_{a0}^m \ \boldsymbol{or}\ H_a L_a^m = H_{a0} L_{a0}^m \quad [3]$$

Fast transient phenomena are often assumed to be adiabatic processes with m = 1.4. The previous work of the authors (Zhou et al., 2013b) investigated the phenomenon of white mist in a rapidly filling pipeline containing an entrapped air pocket numerically and experimentally, and demonstrated that the results with m=1.4 are much closer to the experimental data.

Due to the constant tail water depth, only the interface between the filling water and air pocket is a moving boundary. For the air-water interface, the continuity equation and pressure balance equation can be written as:

$$\frac{dL_f}{dt} = V_w \quad [4]$$

$$H_w = H_a \quad [5]$$

3 SOLUTION TECHNIQUES

3.1 Finite volume methods for the filling water column

FVMs are well-suited for the solution of conservative partial differential equations (PDEs). The system of non-linear hyperbolic equations (Eq. [1] and [2]) can be written in the form:

$$\frac{\partial \mathbf{u}}{\partial t} + \mathbf{A}\frac{\partial \mathbf{u}}{\partial x} = \mathbf{s} \quad [6]$$

where $\mathbf{u} = \begin{pmatrix} H \\ V \end{pmatrix}$; $\mathbf{A} = \begin{pmatrix} V & a^2/g \\ g & V \end{pmatrix}$; and $\mathbf{s} = \begin{pmatrix} 0 \\ -\frac{f|V|V}{2D} \end{pmatrix}$.

The difficulty in solving Eq. [6] is due to the fact that the coefficient matrix **A** depends on the solution vector **u** itself. If the coefficient matrix **A** were to be constant, then the techniques for solving linear hyperbolic systems with constant coefficients.

Here, assume that the initial data and the solution **u** are close to a constant state **ū**. Then, by setting:

$$\bar{\mathbf{A}} \equiv \mathbf{A}(\bar{\mathbf{u}}) \quad [7]$$

Riemann problem for Eq. [6] can be approximated by the Riemann problem for the linear hyperbolic systems with constant coefficients, and Eq. [6] can be treated as the system in conservative form
Therefore, Eq. [6] can be treated as the system in conservative form:

$$\frac{\partial \mathbf{u}}{\partial t} + \frac{\partial \mathbf{f}(\mathbf{u})}{\partial x} = \mathbf{s}(\mathbf{u}), \qquad \mathbf{f}(\mathbf{u}) = \bar{\mathbf{A}}\mathbf{u} \quad [8]$$

where $\bar{\mathbf{A}} = \begin{pmatrix} \bar{V} & a^2/g \\ g & \bar{V} \end{pmatrix}$; and $\bar{V}$=mean value of *V*, which is constant.

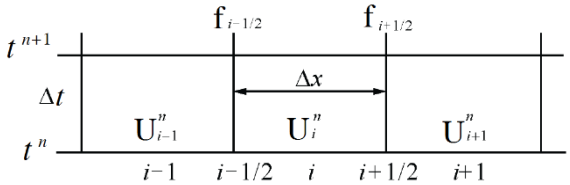

Figure 3. The discretization grids system for the filling water column.

As shown in Figure 3, computational grid involves the discretization of the spatial domain *x* into cells of length Δ*x* and the temporal domain t into intervals of duration Δ*t.* The *i*th control volume is centered at node *i* and extends from *i*-1/2 to *i*+1/2. The flow variables (*H* and *V*) are defined at the cell centers *i* and represent their average value within each cell. Fluxes are calculated at the interfaces between cells (*i*-1/2 and *i*+1/2). For the *i*th cell, the integration of Eq. [8] with respect to *x* from control surfaces *i*-1/2 to *i*+1/2 yields:

$$\frac{\partial}{\partial t}\int_{i-1/2}^{i+1/2}\mathbf{u}dx+\mathbf{f}_{i+1/2}-\mathbf{f}_{i-1/2}=\int_{i-1/2}^{i+1/2}\mathbf{s}dx \quad [9]$$

Because the flow variables are averaged over the cell, the application of $\mathbf{U}_i=\frac{1}{\Delta x}\int_{i-1/2}^{i+1/2}\mathbf{u}dx$ to Eq. [9], gives:

$$\mathbf{U}_i^{n+1}=\mathbf{U}_i^n+\frac{\Delta t}{\Delta x}\left(\mathbf{f}_{i+1/2}-\mathbf{f}_{i-1/2}\right)+\frac{\Delta t}{\Delta x}\int_{i-1/2}^{i+1/2}\mathbf{s}dx \quad [10]$$

where the superscripts *n* and *n*+1 reflect the *t* and *t*+Δ*t* time levels respectively. In Eq. [10], the value of **U** at the new time step *n*+1 requires the computation of the numerical flux at the cell interfaces at the previous time *n* and the evaluation of the source term.

3.2 Computation of flux term by Godunov scheme

In Godunov approach, numerical flux is determined by solving a local Riemann problem at each cell interface. The Riemann problem for a general hyperbolic system is the following initial-value problem (Toro, 2009):

$$\frac{\partial\mathbf{u}}{\partial t}+\frac{\partial\mathbf{f}(\mathbf{u})}{\partial x}=\mathbf{0} \quad [11]$$

$$\mathbf{u}^n(x)=\begin{cases}\mathbf{U}_L^n, & x<x_{i+1/2}\\ \mathbf{U}_R^n, & x>x_{i+1/2}\end{cases} \quad [12]$$

where $\mathbf{U}_L^n$ =average value of **u** to the left of interface *i*+1/2 at *n*; and $\mathbf{U}_R^n$ =average value of **u** to the right of interface *i*+1/2 at *n*.

Simple calculations for the matrix $\bar{\mathbf{A}}$ show that the eigenvalues are:

$$\bar{\lambda_1}=\bar{V}-a,\ \bar{\lambda_2}=\bar{V}+a \quad [13]$$

And the right eigenvectors are:

$$\mathbf{K}^{(1)}=\begin{bmatrix}1\\ -g/a\end{bmatrix}\text{ and }\mathbf{K}^{(2)}=\begin{bmatrix}1\\ g/a\end{bmatrix} \quad [14]$$

As the eigenvectors are linearly independent, expanding the data $\mathbf{U}_L$, constant left state, and $\mathbf{U}_R$, constant right state, as linear combinations of the set $\mathbf{K}^{(1)}$, $\mathbf{K}^{(2)}$, that is:

$$\mathbf{U_L}=\sum_{i=1}^{2}\alpha_i\mathbf{K}^{(i)}\text{ and }\mathbf{U_R}=\sum_{i=1}^{2}\beta_i\mathbf{K}^{(i)} \quad [15]$$

Solving for the four-unknown coefficient α_1, α_2, β_1, β_2, they are:

$$\alpha_1=\frac{1}{2}\left(H_L^n-\frac{a}{g}V_L^n\right),\ \alpha_2=\frac{1}{2}\left(H_L^n+\frac{a}{g}V_L^n\right) \quad [16]$$

$$\beta_1=\frac{1}{2}\left(H_R^n-\frac{a}{g}V_R^n\right),\ \beta_2=\frac{1}{2}\left(H_R^n+\frac{a}{g}V_R^n\right) \quad [17]$$

The general solution to Riemann problem (Eq. [11] and [12]) in terms of the original variables is given as:

$$\mathbf{u}(x,t)=\beta_1\mathbf{K}^{(1)}+\alpha_2\mathbf{K}^{(2)} \quad [18]$$

Now, by using Eq. [18], the exact solution of the variables at the interface *i*+1/2 is:

$$\mathbf{u}_{i+1/2}(t) = \frac{1}{2}\left\{\begin{pmatrix} 1 & a/g \\ g/a & 1 \end{pmatrix}\mathbf{U}_L^n - \begin{pmatrix} -1 & a/g \\ g/a & -1 \end{pmatrix}\mathbf{U}_R^n\right\} \quad [19]$$

Thus, the fluxes at i+1/2 for all internal nodes and for $t_{\in}[\ t^n, t^{n+1}]$ are as follows:

$$\mathbf{f}_{i+1/2} = \bar{\mathbf{A}}_{i+1/2}\mathbf{u}_{i+1/2}(t) = \frac{1}{2}\bar{\mathbf{A}}_{i+1/2}\left\{\begin{pmatrix} 1 & a/g \\ g/a & 1 \end{pmatrix}\mathbf{U}_L^n - \begin{pmatrix} -1 & a/g \\ g/a & -1 \end{pmatrix}\mathbf{U}_R^n\right\} \quad [20]$$

As shown in Eq. [20], for each cell interface, $\mathbf{U}_L^n$ and $\mathbf{U}_R^n$ are estimated from a polynomial reconstruction whose order determines the accuracy of the scheme. For Godunov's first-order accuracy method, a piecewise constant polynomial is used, namely, $\mathbf{U}_L^n = \mathbf{U}_{i+1}^n$ and $\mathbf{U}_R^n = \mathbf{U}_i^n$. In order to compare with the existing elastic models which are all limited to first-order accuracy, only first-order accuracy method was developed here. Godunov's higher order accuracy method will be developed and investigated in the future work.

3.3 Boundary conditions

The implementation of boundary conditions is an important step in solving partial differential equations. The boundary conditions in this model contain the upstream head-constant reservoir and the downstream moving air-water interface.

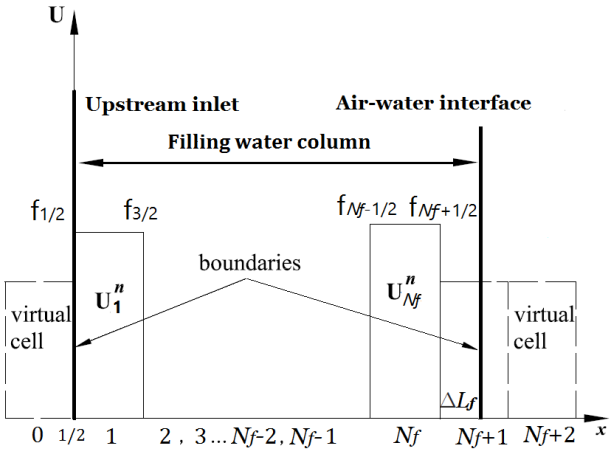

Figure 4. Boundary conditions by adding virtual cells outside the computational domain.

For the computational domain [0, L_f^n] at t=$n\Delta t$, it is discretized into N_f computing cells of length Δx and one smaller cell ΔL_f (here $0<\Delta L_f \leq \Delta x$), and the boundary conditions should be resolved at the boundaries x=0 and x=L_f^n as illustrated in Figure 4. Numerically, such boundary conditions are expected to provide numerical fluxes $\mathbf{f}_{1/2}$, $\mathbf{f}_{Nf+1/2}$ and $\mathbf{u}_{a\text{-}w}$ at the air-water interface. These are required in order to update the extreme cells I_0 and I_{Nf} to the next time level n+1. In this paper, virtual cell I_0 adjacent to I_1, virtual cells I_{Nf+1} and I_{Nf+2} adjacent to I_{Nf}, were used in the upstream and downstream cells of the computational domain. In this way, boundary Riemann problems were solved and the corresponding Godunov fluxes $\mathbf{f}_{1/2}$ and $\mathbf{f}_{Nf+1/2}$ were computed, as done for the interior cells. The imposition of boundary conditions is, fundamentally, a physical problem. It was assumed that the flow information in the virtual cells are the same as those at the boundaries. The numerical implementation for the boundaries are shown as below.

3.3.1 Upstream head-constant reservoir

At the upstream boundary, the Riemann invariant associated with negative characteristic line is:

$$H_{1/2} - \frac{a}{g}V_{1/2} = H_1^n - \frac{a}{g}V_1^n \quad [21]$$

For an upstream reservoir where $H_{1/2} = H_r$, $V_{1/2} = V_1^n + \frac{a}{g}(H_r - H_1^n)$, and the variables at upstream inlet $\mathbf{u}_{1/2}(t) = (H_{1/2}, V_{1/2})$. According to the assumption on the virtual cells, the corresponding values of virtual cell I_0 adjacent to pipeline inlet are:

$$\mathbf{U}_0^{n+1} = \mathbf{u}_{1/2} \quad [22]$$

3.3.2 Strategy of Tracking Air-water Interface

As discussed above, $\mathbf{f}_{Nf+1/2}$ can be obtained from the virtual cells I_{Nf+1} and I_{Nf+2} adjacent to I_{Nf}. At the air-water interface boundary, the Riemann invariant associated with positive characteristic line is:

$$H_{A-W} + \frac{a}{g} V_{A-W} = H_{Nf+1}^{n} + \frac{a}{g} V_{Nf+1}^{n} \quad [23]$$

In the case of partially full pipe in Figure 2, the continuity equation at the surge front yields (Wiggert, 1972; Zhou and Liu, 2013):

$$A \cdot (V_{A-W} - V_w) = A_C \cdot (V_C - V_w) \quad [24]$$

Across the front, momentum is conserved:

$$g \cdot (A_C \cdot H_C - \mathrm{A} \cdot H_{A-W}) = A \cdot (V_{A-W} - V_w) \cdot (V_{A-W} - V_C) \quad [25]$$

$$H_C = H_a + \frac{y_0 \cdot A_C}{A} \quad [26]$$

The experimental observations (can also see in the results of Zhou and Liu (2013)) indicated that tail water was kept to be almost stable during the first air compression. It means that the tail water can be considered as stagnant during the rapid filling process. Namely, the assumption of V_C =0 could be acceptable if the filling is so quick that the surface instability of the tailwater has little time to develop. Substituting V_C =0 into Eq. [24] and [25], the continuity and momentum equations during the first air compression of rapid filling become:

$$A \cdot V_{A-W} = (A - A_C) \cdot V_w \quad [27]$$

$$g \cdot (A_C \cdot H_C - \mathrm{A} \cdot H_{A-W}) + A \cdot V_{A-W} \cdot (V_w - V_C) = 0 \quad [28]$$

Applying the mean value theorem of integrals and the method of mean function in Eq. [4], the equation can be approximated as:

$$L_f = L_f^n + \frac{V_w + V_w^n}{2} \Delta t \quad [29]$$

Combining Eq. [3] and [29], the equation becomes:

$$H_a = H_{a0} \cdot \left(\frac{L_{a0}}{L - L_f^n - \frac{V_w + V_w^n}{2} \Delta t} \right)^m \quad [30]$$

This set of 5 equations (Eq. [23], [26] to [28], and [30]) together with the initial condition constitutes a well posed problem whose solution describes the systems behavior. The goal is to determine the 5 unknown functions: $H_{A\text{-}W}$, $V_{A\text{-}W}$, H_A, H_C and V_w, which can be obtained from the 5 equations.

According to the assumption on the virtual cells, the corresponding values of virtual cells I_{Nf+1} and I_{Nf+2} adjacent to I_{Nf} are:

$$\mathbf{U}_{Nf+1}^{n+1} = \mathbf{U}_{Nf+2}^{n+1} = \begin{pmatrix} H_{A-W} \\ V_{A-W} \end{pmatrix} \quad [31]$$

A rational length extent of ΔL_f (the cell length nearby the air-water interface) is crucial to ensure the calculation accuracy and the performance of the numerical model, so that $0<\Delta L_f \leq \Delta x$ was adopted here. As shown in Figure 4, either $\Delta x<\Delta L_f$ or $\Delta L_f \leq 0$ may occur due to compression or expansion of the air pocket. To validate the assumption of $0<\Delta L_f \leq \Delta x$, a computed node must be added or deleted, estimating the variables at the newly added node by the nearby nodes.

3.4 Incorporation of source terms

The source terms s(u) are introduced into the solution through time splitting using a second-order Runge-Kutta discretization which results in the following explicit procedure.

First step (pure advection):

$$\bar{\mathbf{U}}_i^{n+1} = \mathbf{U}_i^n - \frac{\Delta t}{\Delta x} \left(\mathbf{f}_{i+1/2}^n - \mathbf{f}_{i-1/2}^n \right) \quad [32]$$

Second step (update with source term by Δ*t*/2):

$$\bar{\bar{\mathbf{U}}}_i^{n+1} = \bar{\mathbf{U}}_i^{n+1} + \frac{\Delta t}{2}\mathbf{s}(\bar{\mathbf{U}}_i^{n+1}) \quad [33]$$

Last step (re-update with source term by Δt):

$$\mathbf{U}_i^{n+1} = \bar{\mathbf{U}}_i^{n-1} + \Delta t\mathbf{s}(\bar{\bar{\mathbf{U}}}_i^{n+1}) \quad [34]$$

The Courant number $\mathrm{Cr} = a\Delta t/\Delta x \leq 1$ can satisfy the Courant-Friedrichs-Lewy (CFL) criterion.

4 EXPERIMENTAL PROGRAMS

In order to verify the proposed model, the experiments on the rapid filling of partially full pipe with entrapped air pocket were conducted, as shown in Figure 2. The experimental apparatus and measurement techniques used in this investigation are described carefully in the authors' previous study (Zhou and Liu, 2013).

Total pipe length is 8.824m. Three upstream inlet heads (80, 120 and 160 kPa), three initial air lengths (1.058m, 3.25m and 6.45 m, considering the air entrapped inside of the ball valve), eight varying initial tail water depths (0, 5, 10, 15, 20, 25, 30 and 35 mm) were tested, resulting in a total of 72 test cases. The ball valve was opened as quickly as possible. The wave speed was measured under the rapid valve closure tests with no air. A value of wave speed for the organic glass piping filled was found to be nearly 400m/s. The friction factor under steady-flow conditions, *f*, is determined based on total losses, ranged between 0.075 and 0.095.

5 RESULTS

In this section, the purposes are: (1) to validate the proposed FVM model by comparing the calculated and measured data; and (2) to compare with the existing MOC model developed by Zhou et al. (2013d). In the simulations, the two models both ignore the nonlinear convective terms, meanwhile Courant number Cr=1. Experimental results and the corresponding comparisons of measured and numerical pressures in the entrapped air pocket are shown in Figure 5 and 6.

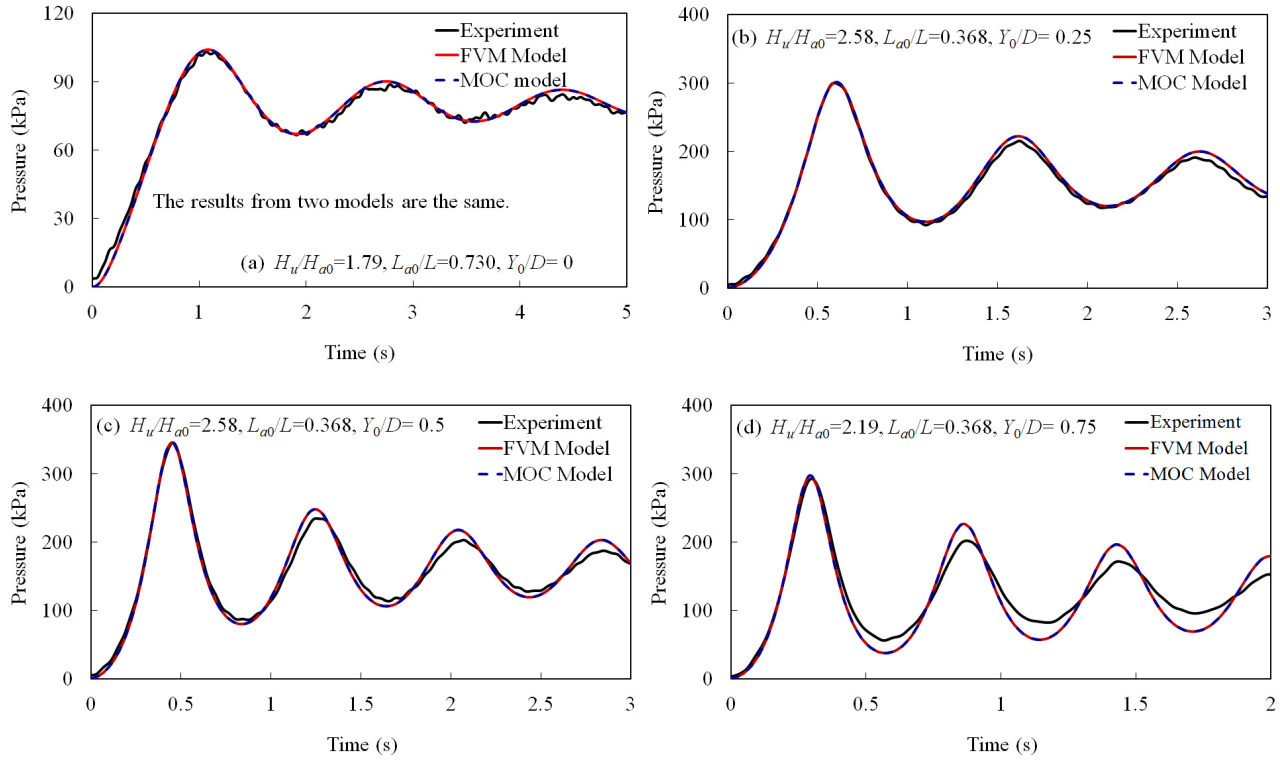

Figure 5. Calculated and measured pressure oscillation patterns with different tail water depth.

5.1 Validation of the proposed FVM model

Figure 5 shows the computed and observed pressure oscillation patterns in the cases with different tail water. For the case without tail water in Figure 5(a), the predicted pressure oscillation patterns are almost consistent with the experimental results. As shown in Figure 5(b-d), for the case with different tail water, the proposed model can still simulated the transient pressures, especially for the first cycle and the frequencies.

However, starting from the second cycle, the peak attenuation is less than that observed in the experiments. One explanation might be that the entrapped air pocket is assumed to remain intact, whereas the air pocket was observed to be broken up by the filling water, especially after the first compression. Another explanation might be the fact that the entrapped air pocket is treated as an ideal gas with a constant polytrophic exponent *m* (*m*=1.4 here), whereas the true dynamic involves a complicated heat transfer process (Zhou et al., 2013b). It is also possible that the constant pipe friction factor would underestimate the pressure peak attenuation (Wylie et al., 1993).

It can also be found in Figure 6 that, for all the experimental cases with different initial air length, tail water depth and driving head, the proposed model would show fairly good overall agreement with experiments in the peak air pressure during the rapid filling process.

Consequently, the proposed model should be a robust tool to simulate the pressure surges in a rapidly filling pipe with tail water and entrapped air pocket, especially the maximum air pressure.

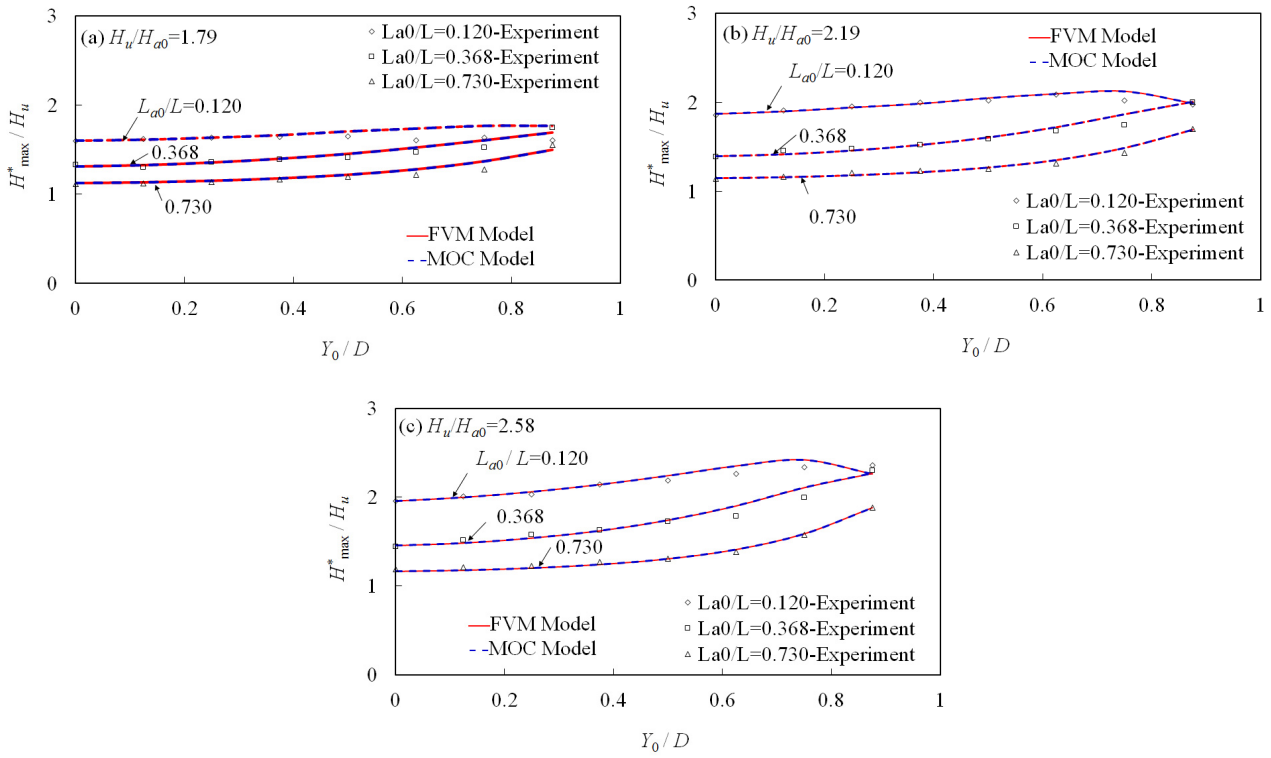

Figure 6. Comparisons between calculated and measured maximum pressure.

5.2 Comparisons between the proposed FVM model and the MOC model

Interestingly, for the same flow conditions, the pressure oscillation patterns and the maximum pressures produced by the proposed FVM model are identical with those predicted by the space-line interpolation fixed-grid MOC scheme (namely, the MOC model), as shown in Figure 5 and 6. Actually, in the pipe flow with only water phase (pure water hammer flow), Zhao and Ghidaoui (2004) have demonstrated that the first-order Godunov scheme and the MOC with space-line interpolation scheme are identical in the case of water hammer. In order to explain, in this paper, assuming pipe friction is zero, we can obtain from Eq. [32] to [34]:

$$\mathbf{U}_i^{n+1} = \mathbf{U}_i^n - \frac{\Delta t}{\Delta x}\left(\mathbf{f}_{i+1/2}^n - \mathbf{f}_{i-1/2}^n\right) \quad [35]$$

Since that the nonlinear convective terms are neglected and Courant number $a\Delta t/\Delta x$=1, the first-order Godunov scheme, obtained by inserting Eq. [35] into Eq. [20], is as follows:

$$\mathbf{H}_i^{n+1} = \frac{1}{2}\left[(\mathbf{H}_{i-1}^n + \mathbf{H}_{i+1}^n) - \frac{a}{g}(\mathbf{V}_{i-1}^n - \mathbf{V}_{i+1}^n)\right] \quad [36]$$

$$\mathbf{V}_i^{n+1} = \frac{1}{2}\left[(\mathbf{V}_{i-1}^n + \mathbf{V}_{i+1}^n) - \frac{a}{g}(\mathbf{V}_{i-1}^n - \mathbf{V}_{i+1}^n)\right] \quad [37]$$

It can be found that Eq. [36] and [37] are identical with the MOC with space-line interpolation scheme developed by Wylie et al. (1993), explaining the excellent agreement between the two schemes.

6 CONCLUSIONS

The transient flow with entrapped air pocket often happens in water pipelines. So far, the simulations for elastic water column in the rapid filling pipeline are almost treated as the classical water hammer problem, and the related numerical scheme is the fixed-grid MOC. In this paper, first-order explicit FV Godunov-type scheme was developed to handle the air-water problem in the rapid filling pipeline. Comparisons of the experimental data and the results calculated by the proposed FVM model and the previous MOC model were conducted. Results indicate that the proposed model should be a robust tool to simulate the pressure surges in a rapidly filling pipe with tail water and entrapped air pocket, especially the maximum air pressure. Moreover, for the same flow conditions, the pressure oscillation patterns and the maximum pressures produced by the proposed FVM model are identical with those predicted by the MOC model.

In the future work, the accuracy of FVM Godunov-type schemes will be raised by incorporating the high-resolution techniques such as limiters into the solution of water hammer problems, to simulate the transient pressure in the rapid filling pipe with entrapped air pocket.

ACKNOWLEDGEMENTS

The writers gratefully acknowledge the financial support for this research from the National Natural Science Foundation of China (Grant No. 51679066 and 51209073), the Fundamental Research Funds for the Central Universities (Grant No. 2015B15414), and Open Research Fund Program of State Key Laboratory of Water Resources and Hydropower Engineering Science (Grant No. 2016SDG01)

NOTATIONS

The following symbols are used in this paper:

a = wavespeed (m/s)
A = cross-sectional area of pipe section (m^2)
A = coefficient matrix (-)
A_C = the tailwater wet area (m^2)
Cr=Courant number (-)
D = the pipe diameter (m)
f = pipe wall friction coefficient
g = gravitational acceleration (m/s^2)
H = piezometric head (m)
H_a = absolute pressure head of air pocket (m)
H_{a0} = initial absolute pressure head of air pocket (m)
$H_{A\text{-}W}$ = the pressure head upstream side of the surge front (m)
H_C = the pressure head downstream side of the surge front (m)
H_r = the upstream (gauge) head (m)
H_u = the absolute upstream head (m)
H_w = pressure head at the surge front at t time (m)
I_i = the cell in computation region (-)
$\mathbf{K}^{(i)}$ = the right eigenvectors of the matrix $\overline{\mathbf{A}}$
L_a = length of entrapped air pocket (m)
L_{a0} = initial length of entrapped air pocket (m)
L_f = filling water column length at t time (m)
L_{f0} = the initial length of filling water column (m)
N_f = the cell number of filling water column (m)
t = time (s)
u = solution vector (-)
$\mathbf{U}_L^n$ =average value of **u** to the left of interface i+1/2 at n (-)
$\mathbf{U}_R^n$ =average value of **u** to the right of interface i+1/2 at n (-)
V = the average cross-sectional velocity (m/s)
$\bar{V}$ = mean value of V (m/s)
V_a = volume of entrapped air pocket (m^3)
V_{a0} = initial volume of entrapped air pocket (m^3)
$V_{A\text{-}W}$ = the velocity of filling column end (m/s)
V_C = the velocity of tailwater (m/s)
V_w = the velocity of surge front (m/s)
x = distance along pipeline (m)

y_0 = the centroidal depth of tail water (m)
Y_0 = initial tail water depth (m)
Δx = length of cell (m)
Δt = time step increment (s)
Δ_i = the slope vector (-)
ΔL_f = the cell length nearby the air-water interface (-), and
$\bar{\lambda}$= the eigenvalues of the matrix $\bar{\mathbf{A}}$ (-).

REFERENCES

BHR Group. (2015). Guideline and Introduction. *12th Int. Conf. Pressure Surges*, Dublin, November 18-20 2015.(www.bhrconferences.com)

Cabrera, E., Abreu, J., Perez, R. & Vela, A. (1992). Influence of Liquid Length Variation in Hydraulic Transients. *Journal of Hydraulic Engineering,* 118(12), 1639-1650.

Guinot, V. (2001). Numerical Simulation of Two-Phase Flow in Pipes Using Godunov Method. *Int. J. Numer. Meth. Eng.,* 50(5), 1169-1189.

Hou Q., Tijsseling A., Laanearu J., Annus I., Koppel T., Bergant A., Vuckovic S., Anderson A. & Westende J. (2014). Experimental Investigation on Rapid Filling of a Large-Scale Pipeline. *Journal of Hydraulic Engineering,* 140(11), 04014053.

Hwang, Y.H. & Chung, N.M. (2002). A Fast Godunov Method for The Water-Hammer Problem. *International Journal of Numerica Methods Fluids.,* 40(6), 799-819.

Izquierdo, J., Fuertes, V. S., Cabrera, E., Iglesias, P. L. & Garcia-Serra, J. (1999). Pipeline Start-Up with Entrapped Air. *Journal of Hydraulic Research,* 37(5), 579-590.

Lee, N.H. & Martin, C.S. (1999) Experimental and Analytical Investigation of Entrapped Air in a Horizontal Pipe. *Proc. of the 3rd ASME/JSME Joint Fluids Engineering Conference*, San Francisco, California, 1-8.

Leon, A.S., Ghidaoui, M.S., Schmidt, A.R. & Garcia, M.H. (2006). Godunov-Type Solutions for Transient Flows in Sewers. *Journal of Hydraulic Engineering,* 132(8), 800-813.

Leon, A.S., Ghidaoui, M.S., Schmidt, A.R. & Garcia, M.H. (2010). A Robust Two-Equation Model for Transient-Mixed Flows. *Journal of Hydraulic Engineering,* 48(1), 44-56.

Liu, D., Zhou, L., Karney, B., Zhang, Q. & Ou, C. (2011). Rigid-plug Elastic-Water Model for Transient Pipe Flow with Entrapped Air Pocket. *Journal of Hydraulic Research,* 49(6), 799-803.

Malekpour, A. (2014). Analysis of Rapid Pipeline Filling Including Column Separation & Entrapped Air Effects. *PhD Thesis*, University of Toronto, Department of Civil Engineering.

Martin, C.S. (1976). Entrapped Air in Pipelines. *Int. Conf. on pressure surges*, BHRA, England, London, 15-27.

Toro, E.F. (2009). *Riemann Solvers and Numerical Methods for Fluid Dynamics: A Practical Introduction.* Springer-Verlag Berlin Heidelberg, Dordrecht Heidelberg London New York.

Wiggert, D.C. (1972). Transient Flow in Free-surface, Pressurized Systems. *Journal of Hydraulic Division* 98(HY1), 11-27.

Wylie, E.B., Streeter, V.L. & Suo, L.S. (1993). *Fluid Transients in Systems.* Prentice Hall, New York.

Zhao, M. and Ghidaoui, M. (2004). Godunov-Type Solutions for Water Hammer Flows. *Journal of Hydraulic Engineering,* 130(4), 341-348.

Zhou, F., Hicks, F.E. & Steffler, P.M. (2002). Transient Flow in a Rapidly Filling Horizontal Pipe Containing Trapped Air. *Journal of Hydraulic Engineering*,128(6), 625-634.

Zhou, L. & Liu, D. (2013). Experimental Investigation of Entrapped Air Pocket in a Partially Full Water Pipe. *Jornal of Hydraulic Research,* 51(4), 469-474.

Zhou, L., Liu, D. & Karney, B. (2013a). Investigation of Hydraulic Transients of Two Entrapped Air Pockets in a Water Pipeline. *Journal of Hydraulic Engineering,* 139(9), 949-959.

Zhou, L., Liu, D., Karney, B. & Wang, P. (2013b). Phenomenon of White Mist in Pipelines Rapidly Filling with Water with Entrapped Air Pockets. *Journal of Hydraulic Engineering,* 139(10), 1041-1051.

Zhou, L., Liu, D., Karney, B. & Zhang, Q. (2011a). Influence of Entrapped Air Pockets on Hydraulic Transients in Water Pipelines. *Journal Hydraulic Engineering,* 137(12), 1686-1692.

Zhou, L., Liu, D., Karney, B. & Zhang, Q. (2013c). Closure to “Influence of Entrapped Air Pockets on Hydraulic Transients in Water Pipelines”. *Journal of Hydraulic Engineering,* 139(1), 107-108.

Zhou, L., Liu, D. & Ou, C. (2011b). Simulation of Flow Transients in a Water Filling Pipe Containing Entrapped Air Pocket with VOF Model. *Journal Engineering Applications of Computational Fluid Mechanics,* 5(1): 127-140.

Zhou, L., Liu, D. & Xia, L. (2013d). Partially Full Model for Transients in Rapidly Filling Pipe with Trapped Air. *2013 IAHR World Congress*. Tsinghua University, Chengdu, China.

